Journal of Alloys and Compounds 505 (2010) 505–509

Contents lists available at ScienceDirect

Journal of Alloys and Compounds

journal homepage: www.elsevier.com/locate/jallcom

Effect of heat treatment on the highly corrosion-resistant $Cu_{70}Ni_{27.7}Fe_{2.3}$ alloy

Zhang Jie, Wang Qing*, Wang Yingmin, Wen Lishi, Dong Chuang

Key Laboratory of Materials Modification by Laser, Ion and Electron Beams, School of Materials Science & Engineering, Dalian University of Technology, Dalian 116024, China

ARTICLE INFO

Article history:
Received 30 January 2010
Received in revised form 11 May 2010
Accepted 28 June 2010
Available online 3 July 2010

Keywords:
Cu–Ni
Heat treatment
Cluster model
Corrosion

ABSTRACT

Minor Fe additions are widely added to enhance the corrosion resistance of cupronickel alloys. The present paper aims at optimizing the amounts of Fe in $Cu_{70}(Ni,Fe)_{30}$ (at.%) alloys using a cluster-plus-glue-atom model for stable solid solutions. By this model, it is assumed that one Fe atom and 12 Ni atoms formed a Fe-centered and Ni-surrounded cube-octahedron cluster and the isolated $FeNi_{12}$ clusters embedded in a Cu matrix. The stable solid solution alloy composition of Fe-modified $Cu_{70}Ni_{30}$ alloy was described by a cluster formula $[Fe_1Ni_{12}]Cu_{30.3} = Cu_{70}Ni_{27.7}Fe_{2.3}$ (at.%). The effect of homogenizing annealing treatment on the microstructure and corrosion resistance was also investigated by XRD, TEM and electrochemical corrosion measurements. The corrosion test indicates that the $Cu_{70}Ni_{27.7}Fe_{2.3}$ alloy annealed at 800 °C for 5 h possesses the best corrosion resistance in 3.5% NaCl solution.

1. Introduction

The 70/30 Cu–Ni alloys are widely employed as heat exchanger tube and vessel materials due to their good resistance to seawater corrosion [1–3]. The addition of minor Fe to Cu–Ni alloys was found to be particularly beneficial to enhance the corrosion resistance, and a synergistic effect of Ni and Fe on sea water corrosion behavior was also found [4–6]. The Fe–Ni precipitates deteriorate the corrosion performance when the Fe content exceeds 2 at.% in the Cu–Ni alloys containing 10 wt.% Ni [7–8]. It was demonstrated that the mechanical properties of Cu–Ni alloys were influenced by heat treatment [9–10]. Although much research has been devoted to the corrosion behavior of Cu–Ni alloys in seawater, the Fe contents in $Cu_{70}Ni_{30}$ alloys and the influence of annealing treatment on the microstructure and corrosion behavior of Cu–Ni alloys remain unresolved.

The aim of the present investigation was two-fold, first to theoretically optimize the Fe levels in $Cu_{70}Ni_{30}$ alloys from the view point of an atomic cluster structure model for stable solid solution, and second to experimentally investigate the effect of the heat treatments on the microstructure and the corrosion resistance of $Cu_{70}(Ni,Fe)_{30}$ (at.%) alloys.

2. Composition design

In an alloy containing elements with negative enthalpies of mixing ($\Delta H < 0$), dissimilar atoms tend to form nearest neighbors and the resultant nearest neighbor local atomic environments are characteristic of this alloy structure. These nearest neighbor coordination polyhedra, called atomic clusters in the present paper, have been used to explore the composition rules of metallic glasses and quasicrystals [11–12]. For instance, a Cu-centered Cu_8Zr_5 icosahedron, derived from a devitrification phase Cu_8Zr_3, explains a series of Cu–Zr-based metallic glasses. It was then proposed that compositions with high glass-forming abilities satisfied a simple and universal formula $(cluster)_1(glue\ atom)_x$, $x \approx 1$ or 3. This cluster-based description, termed the cluster-plus-glue-atom model, suggests a new way of understanding atomic structures: a metallic glass can be viewed as a random and dense packing of a certain cluster glued with one or three third element situated in the interstitial sites between the clusters. Such an idea is essentially similar to Miracle's sphere packing scheme for metallic glasses [13], where atomic clusters centered by primary solute atoms are densely packed in a face-centered-cubic-like (FCC-like) structure for $CN \geq 12$ clusters, *CN* being the coordination number of the clusters.

The very same idea can be generalized to solid solutions composed of elements showing negative enthalpies of mixing. A solute atom should be preferentially surrounded by the solvent ones. The solid solution structure can be viewed as random packings of solute-centered and solvent-surrounded clusters. This constitutes a unique structure description alternative to the conventional unit cell one. Only the nearest neighbor interactions are involved in this simplified scheme.

The atomic size differences of Cu, Ni, and Fe are negligibly small so that any chemical effect can be easily manifested as resulted from enthalpies of mixing. Cu and Ni atoms show a small positive enthalpy of mixing ($\Delta H_{Cu-Ni} = 4$ kJ/mol [14]). A relatively large and

* Corresponding author. Fax: +86 411 84708615.
E-mail address: wangq@dlut.edu.cn (W. Qing).

0925-8388/$ – see front matter © 2010 Elsevier B.V. All rights reserved.
doi:10.1016/j.jallcom.2010.06.148

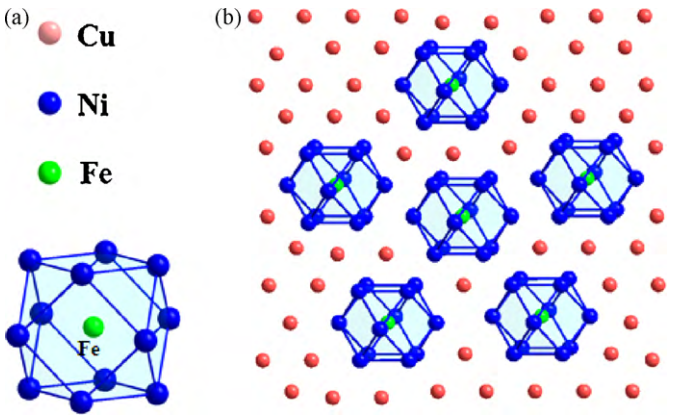

Fig. 1. Cluster-plus-glue-atom model of FCC Cu–Ni–Fe solid solution alloys, (a) Fe_1Ni_{12} cube-octahedral cluster, (b) $FeNi_{12}$ clusters embedded in a Cu matrix.

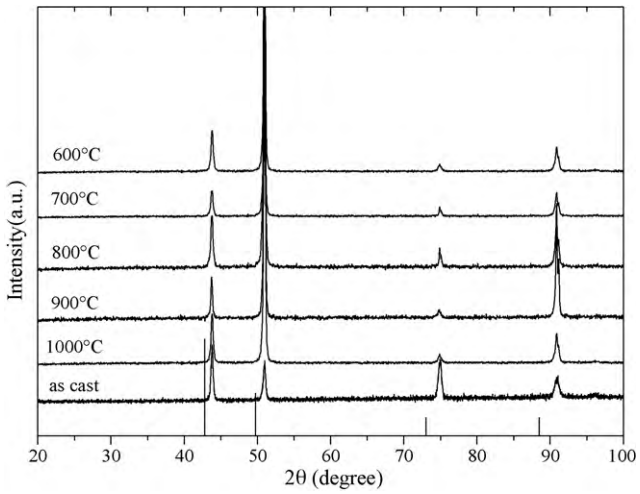

Fig. 2. XRD patterns of $Cu_{70}Ni_{27.7}Fe_{2.3}$ alloy annealed at different temperatures.

positive enthalpy of mixing between Cu and Fe (ΔH_{Cu-Fe} = 13 kJ/mol [14]) indicates that Cu tends to separate from Fe upon mixing. Fe and Ni, however, exhibit a small negative enthalpy of mixing H_{Fe-Ni} = −2 kJ/mol [14]. They are miscible at all proportions at high temperatures, but undergo a eutectoid reaction at low temperatures. Therefore, Fe–Ni dissimilar bonding is preferred against Fe–Fe and Ni–Ni ones in the Fe–Ni FCC solid solutions, which promotes the Fe–Ni-type short-range order. In the ideal case, one Fe atom would be screened completely by 12 solvent Ni atoms, forming cube-octahedron Fe_1Ni_{12} (Fig. 1a). In order to avoid the occurrence of any longer-range ordering Ni–Fe–Ni–Fe, ... in the lattice that eventually leads to the $FeNi_3$ phase, the $FeNi_{12}$ clusters would not allow any sharing with their neighboring clusters and this is the case of the solid solubility at which the Fe/Ni proportion is the same as the cluster itself, viz. Fe:Ni = 1:12. In another paper, we illustrated how our cluster structure model is applied to analyze the solubility of Fe in Fe-modified $Cu_{70}Ni_{30}$ FCC stable solid solution alloy [15–16]. The overall atomic structure of the Cu–Ni–Fe FCC substitutional solid solution is thus viewed as Fe-centered and Ni-surrounded $FeNi_{12}$ cube-octahedra embedded in Cu matrix as shown schematically in Fig. 1b.

From the above analysis, The stable solid solution composition of the Fe-modified $Cu_{70}Ni_{30}$ alloys is described by $Cu_{70}Ni_{27.7}Fe_{2.3}$ (at.%), or in cluster formal $[Fe_1Ni_{12}]Cu_{30.3}$. The Fe content of 2.3% (or 2.1 wt.%) is within the Fe content range of 0.4–2.3 wt.% for commercial alloys such as Cu–30%Ni–1%Fe [UNS C71500] and Cu–30%Ni–2%Fe [UNS C71640] [17].

3. Experimental

3.1. Materials preparation

Fe-modified $Cu_{70}Ni_{27.7}Fe_{2.3}$ alloy was prepared by arc melting in a water-chilled copper crucible under an argon atmosphere. The metal purities are 99.99 wt.% for Cu, 99.99 wt.% for Ni and 99.99 wt.% for Fe respectively. The initial vacuum level in the chamber was about 5×10^{-3} Pa. The ingots were annealed for 5 h at 1000, 900, 800, 700 and 600 °C in an annealing furnace, and subsequently quenched in water.

3.2. Materials characterization

Phase identification was carried out by means of XRD (Cu Kα radiation, λ = 0.15406 nm). The standard twin-jet electrolyte thinning was employed to prepare TEM specimens. The sample thinning processes were accomplished in a bath containing 75% CH_3OH and 25% HNO_3 (volume fraction) at −40 °C. TEM observations were carried out on a TECNAI G20-STWIN TEM operated at 200 kV.

Corrosion resistances in a 3.5% NaCl solution were measured to simulate the sea water corrosion. Electrochemical measurements were performed in a typical three-electrode electrochemical cell with saturated calomel as the reference electrode and a platinum sheet as the counter electrode at room temperature.

The weight loss method was used to evaluate the general corrosion behavior. Samples for immersion test were first ground with SiC papers and then polished. The as-polished samples were ultrasonically cleaned for the subsequent weight loss tests. The samples were immersed in a 3.5% NaCl solution at room temperature for different times. The sample weights before and after corrosion were measured with an accuracy of $\pm 5 \times 10^{-4}$ g. Corrosion rates were calculated from $\nu = (w_1 - w_2)/(D \times S \times t)$, where ν is the corrosion rate (μm/h), D the density of the alloy (g cm^{-3}), S the area of specimen surface (cm^2), and t the immersion time (h).

4. Results and discussions

4.1. Microstructure

The microstructure is first analyzed by XRD measurement. Fig. 2 shows the XRD patterns of the $Cu_{70}Ni_{27.7}Fe_{2.3}$ alloy as cast and annealed at different temperature for 5 h and then quenched in water. The XRD patterns can be indexed by an FCC solid solution alloy structure. As compared with the diffraction peak positions of pure Cu metal, the peaks of these solid solution alloys shift to higher diffraction angles, indicating solid solution of Fe and Ni in Cu.

In order to reveal the microstructure influenced by the heat treatments, the $Cu_{70}(Ni,Fe)_{30}$ alloy was analyzed by SEM and TEM.

The SEM micrographs of the $Cu_{70}Ni_{27.7}Fe_{2.3}$ alloy annealed at 600–1000 °C are shown in Fig. 3. The as-cast alloy presents a typical dendrite structure as shown in Fig. 3(a). The examinations of the sample annealed at 1000 and 900 °C and then quenched in water revealed a single phase, but with grain sizes ranging from 100 to 400 μm as shown in Fig. 3(b) and (c), and the dendrite microstructure has disappeared. This inhomogeneous grain size distribution is typical of a recrystallization structure during the cooling process. The examinations of the sample annealed at 800, 700 and 600 °C and then quenched in water revealed a macroscopically homogeneous single-phase structure, with much narrower grain size ranges, about 150 μm, as shown in Fig. 3(d)–(f).

Fig. 4 shows bright-field TEM images and selected area diffraction patterns of the $Cu_{70}Ni_{27.7}Fe_{2.3}$ alloy annealed at 1000, 800 and 600 °C for 5 h and then quenched in water (the structure of the 900 °C-annealed sample is similar to that of 1000 °C and is not shown). Though a single-phase solid solution structure is always retained, significant fluctuation contrasts of unknown origin appear in both the high temperature (1000 °C) and low temperature (600 °C) samples, and such inhomogeneous structures are related to negated corrosion resistance performance of these samples in comparison with the 800 °C-annealed one as will be shown in the next section.

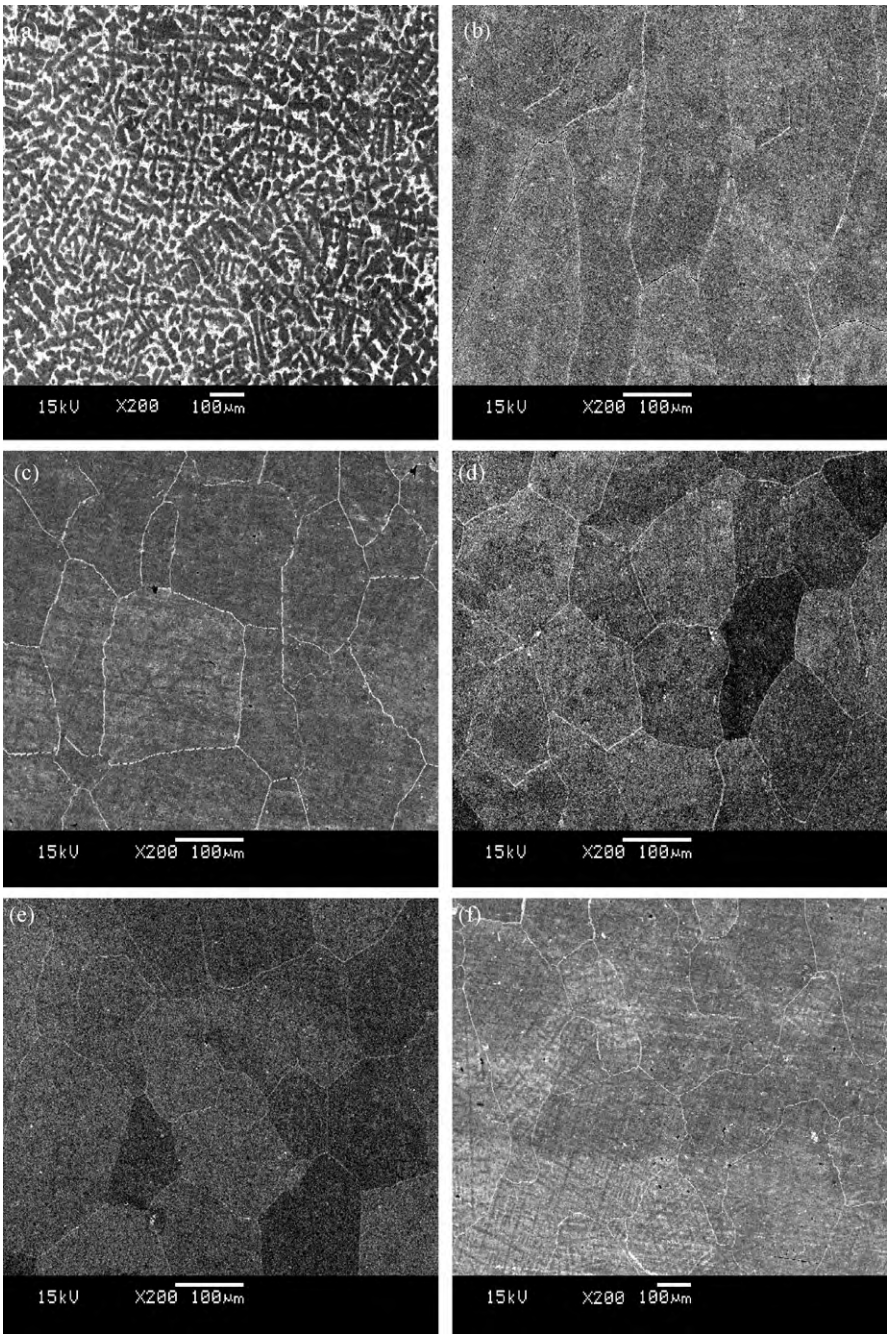

Fig. 3. SEM micrographs of $Cu_{70}Ni_{27.7}Fe_{2.3}$ alloy as cast (a), annealed at 1000 °C (b), 900 °C (c), 800 °C (d), 700 °C (e) and 600 °C (f).

4.2. Corrosion measurement

Based on the above XRD and TEM structural analysis, it is concluded that it is a single homogeneous phase for the $Cu_{70}Ni_{27.7}Fe_{2.3}$ alloy annealed at 800–900 °C for 5 h and then quenched in water, to contrast with the 1000 °C-annealed sample possessing a recrystallization-like structure and with the lower temperature-annealed samples showing a possible spinodal decomposition tendency. In the following, the corrosion resistance results are presented to reveal the corrosion performances as influenced by the heat treatments.

Fig. 5 shows room-temperature potentiodynamic polarization curves of the $Cu_{70}Ni_{27.7}Fe_{2.3}$ alloy annealed at different temperatures and then quenched in water. To further quantitatively study the polarization curves in Fig. 5, a plot was analyzed by Tafel extrapolation. Parameters such as cathodic (β_c) and anodic (β_a) Tafel slopes, corrosion current density (i_{corr}) and corrosion potential (E_{corr}) were calculated and tabulated in Table 1.

Fig. 6 shows the variations of corrosion current density i_{corr} and corrosion potential E_{corr} of $Cu_{70}Ni_{27.7}Fe_{2.3}$ stable solid solution alloy as a function of the annealed temperature. The i_{corr} of as-cast $Cu_{70}Ni_{27.7}Fe_{2.3}$ alloy is 178.1 μA cm^{-2}. However, it sharply decreases to 10.9 μA cm^{-2} for the $Cu_{70}Ni_{27.7}Fe_{2.3}$ alloy annealed at 800 °C for 5 h, which exhibits the lowest i_{corr} and the highest E_{corr} value nearly and shows the best corrosion resistance.

The corrosion resistances changes of $Cu_{70}Ni_{27.7}Fe_{2.3}$ alloy can be partly explained using the microstructure evidence revealed by SEM and TEM. The homogeneous 800 °C-annealed $Cu_{70}Ni_{27.7}Fe_{2.3}$

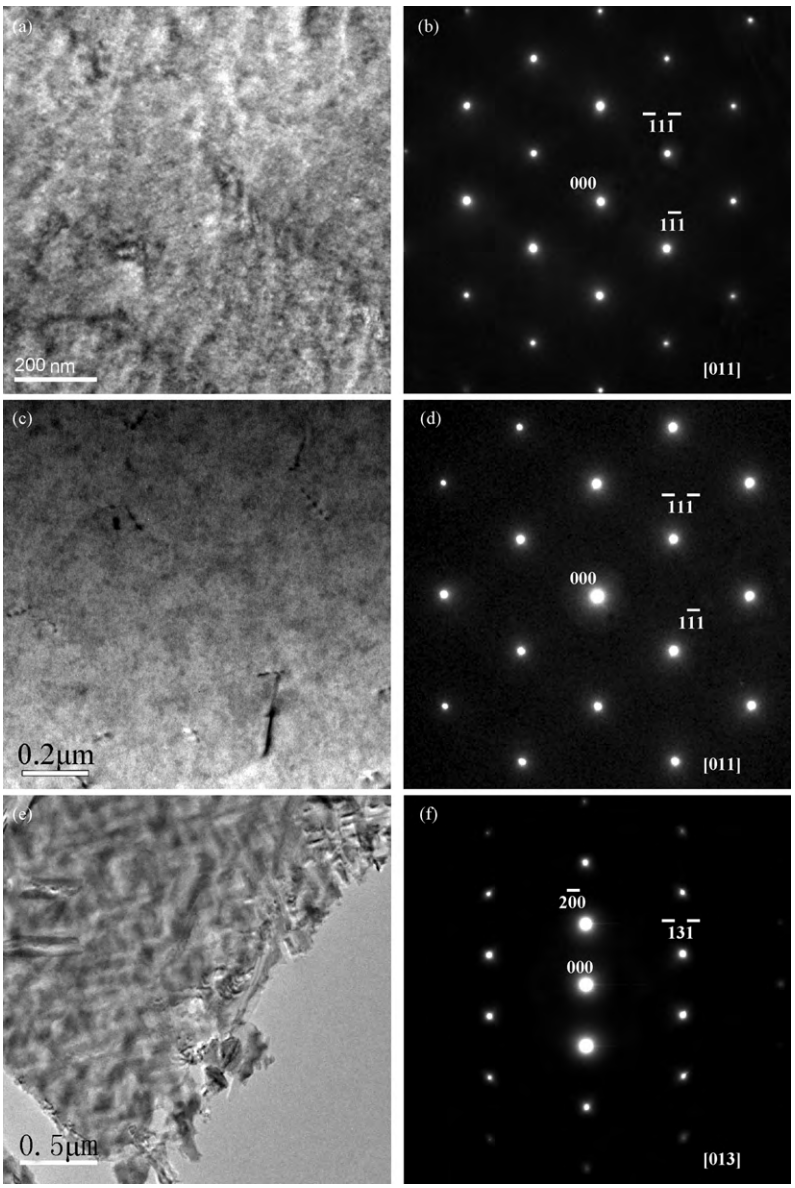

Fig. 4. TEM images and selected area diffraction patterns of $Cu_{70}Ni_{27.7}Fe_{2.3}$ alloy annealed at 1000 °C (a and b), 800 °C (c and d), and 600 °C (e and f).

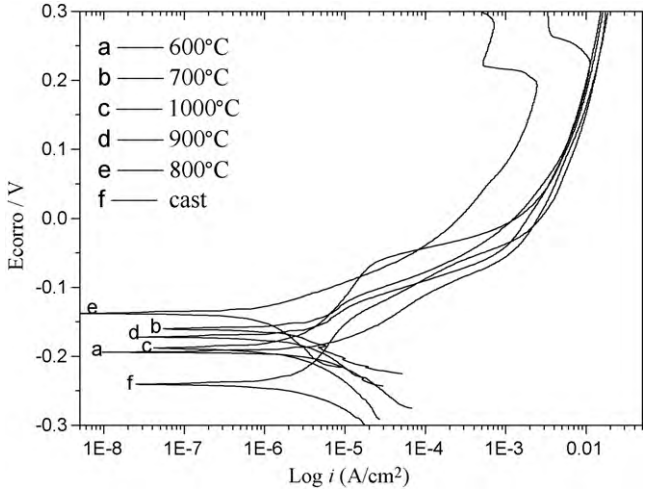

Fig. 5. Comparison of potentiodynamic polarization curves of the $Cu_{70}Ni_{27.7}Fe_{2.3}$ alloy in 3.5% NaCl.

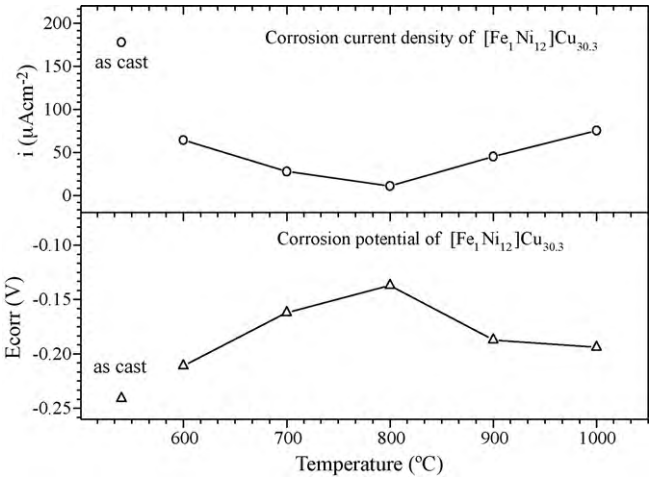

Fig. 6. Variation of corrosion current density and corrosion potential vs. heat treatment temperature.

Table 1
Tafel analysis of polarization curves of the $Cu_{70}Ni_{27.7}Fe_{2.3}$ alloy in 3.5% NaCl solution obtained by fitting the curves in Fig. 5.

Anneal temperature	E_{corr} (V)	i_{corr} ($\mu A\,cm^{-2}$)	β_a ($V\,dec^{-1}$)	β_c ($V\,dec^{-1}$)
As cast	−0.241	178.1	0.233	−0.154
1000 °C	−0.181	34.3	0.194	−0.139
900 °C	−0.162	30.7	0.156	−0.143
800 °C	−0.137	10.9	0.126	−0.141
700 °C	−0.157	45.3	0.172	−0.132
600 °C	−0.184	75.51	0.195	−0.125

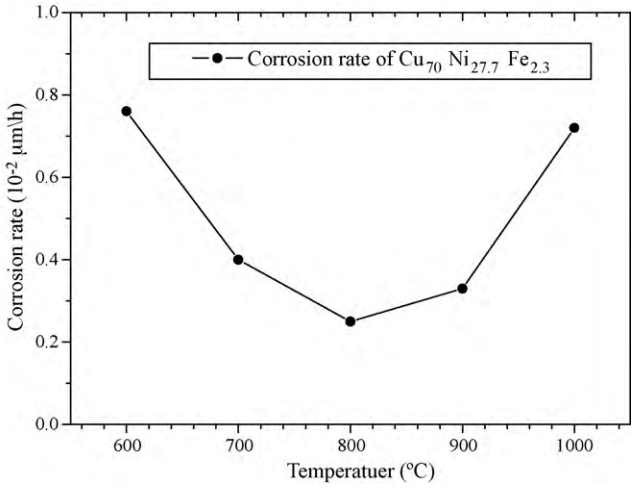

Fig. 7. Static immersion corrosion rates vs. heat treatment temperature.

solid solution alloy possesses the best corrosion resistance. The corrosion resistance of the sample annealed at other temperatures decreases probably owing to the fluctuation-like inhomogeneities.

Fig. 7 shows the static immersion corrosion rates of all alloys annealed at different temperatures in the 3.5% NaCl solution for 240 h. It can be seen that the corrosion rate decreases with the increase in annealing temperature up to 800 °C, followed by an increasing trend. The $Cu_{70}Ni_{27.7}Fe_{2.3}$ alloy annealed at 800 °C and then quenched in water has the best corrosion resistance in the 3.5% NaCl aqueous solution. This is in agreement with the results of electrochemical measurements. The corrosion rate decreases with the annealing temperature due to the difference in microstructure. The average corrosion rate of the $Cu_{70}Ni_{27.7}Fe_{2.3}$ alloy in the 3.5% NaCl solution is about 0.0025 μm/h.

5. Conclusions

A composition formula $[Fe_1Ni_{12}]Cu_{30.3} = Cu_{70}Ni_{27.7}Fe_{2.3}$ (at.%) is pointed out for the $Cu_{70}(Ni,Fe)_{30}$ (at.%) alloy by using a cluster-based stable solid solution model. By this model, it is assumed that one Fe atom and 12 Ni atoms formed an Fe-centered and Ni-surrounded cube-octahedron cluster and the isolated $FeNi_{12}$ clusters embedded in a Cu matrix. The designed alloy $Cu_{70}Ni_{27.7}Fe_{2.3}$ annealed at 800 °C for 5 h possesses a homogeneous structure and hence the best corrosion resistance in a 3.5% NaCl aqueous solution, and the static immersion corrosion rate is 0.0025 μm/h.

Acknowledgements

This project is supported by the National Science Foundation of China (no. 50901012) and by the National Basic Research Program of China (no. 2007CB613902).

References

[1] D.D. Marsden, Mater. Perform. 17 (1978) 9–12.
[2] C. Pearson, Br. Corros J. 7 (1972) 61–68.
[3] L.J.P. Drolenga, F.P. Ijsseling, B.H. Kolster, Mater. Corros. 34 (1983) 167–178.
[4] W.C. Stewart, F.L. La Que, Corrosion 8 (1952) 259–277.
[5] R.F. North, M.J. Pryor, Corros. Sci. 10 (1970) 297–311.
[6] K.D. Efird, Corrosion 33 (1977) 347–351.
[7] G.L. Bailey, J. Inst. Met. 79 (1951) 243–292.
[8] J.M. Popplewell, R.J. Hart, J.A. Ford, Corros. Sci. 13 (1973) 295–309.
[9] A.M. Beccaria, G. Poggi, Y.Z. Wang, Mater. Corros. 45 (1994) 562–569.
[10] X. Mao, F. Fang, F. Yang, J. Jiang, R. Tan, J. Mater. Process Technol. 209 (2009) 2145–2151.
[11] C. Dong, Q. Wang, J.B. Qiang, Y.M. Wang, N. Jiang, G. Han, Y.H. Li, J. Wu, J.H. Xia, J. Phys. D: Appl. Phys. 40 (2007) R273–R291.
[12] C. Dong, W.R. Chen, Y.M. Wang, J.B. Qiang, Q. Wang, Y. Lei, M. Calvo-Dahlborg, J.M. Dubois, J. Non-Cryst. Solids 353 (2007) 3405–3411.
[13] D.B. Miracle, Acta Mater. 54 (2006) 4317–4336.
[14] A. Takeuchi, A. Inoue, Mater. Trans. JIM 41 (2000) 1372–1378.
[15] J. Zhang, Q. Wang, Y.M. Wang, C.Y. Li, L.S. Wen, C. Dong, J. Mater. Res. 25 (2010) 328–336.
[16] J. Zhang, Q. Wang, Y.M. Wang, C. Dong, Acta Metal. Sin. 45 (2009) 1390–1395.
[17] A.J. Sedriks, Mater. Perf. 33 (1994) 56–63.